NPL REPORT MOT 10

REPORT

# Design of two systems to measure the phase change at reflection and one system to measure the variability in contact error due to wringing

Richard K Leach, Keith Jackson and Anne Hart

APRIL 1997

NPL
National Physical Laboratory

NPL Report MOT 10

April 1997

# Design of two systems to measure the phase change at reflection and one system to measure the variability in contact error due to wringing

Richard K Leach, Keith Jackson and Anne Hart
Centre for Mechanical and Optical Technology
National Physical Laboratory
Queens Road
Teddington
Middlesex
United Kingdom
TW11 0LW

**Abstract**

When measuring the length of a gauge block by optical interferometry, the phase changes at reflection from the gauge block and the platen surfaces differ. This difference can give rise to an error in the measured length. There is also an effective phase change at reflection caused by the surface roughness of the gauge and platen causing the reflected wave to appear to come from a surface below that which would be measured with a mechanical comparator. Another source of error in gauge block metrology is the variability in the contact distance caused by the necessity to wring a gauge to the platen. This report outlines the design of two systems that measure the correction for the effect of the phase change at reflection and one system that measures the variability in the contact distance due to wringing.

ISSN 1361-4088

National Physical Laboratory
Queens Road, Teddington, Middlesex, United Kingdom, TW11 0LW



Approved on behalf of the Managing Director
by Dr A R Colclough, Director of Centre for Mechanical and Optical Technology

# CONTENTS

# FIGURE LEGENDS

## 1 INTRODUCTION

The purpose of this report is to summarise the results of detailed theoretical and experimental studies into the phenomena of the phase change at reflection and the wringing effect, and to outline designs of instruments to measure them. Both of these complex phenomena cause uncertainty when measuring the length of an end standard by wringing it to an auxiliary plate (platen) and using optical interferometry (Pugh and Jackson 1986).

It has been found that the dominant parameter that effects the phase change at reflection is surface roughness. When an electromagnetic wave is reflected from a surface the effective plane of reflection is situated around the middle of the roughness profile. This plane of reflection causes a difference between optical and mechanical length measurements. Optical constants and other physical phenomena (dispersion, presence of thin films, *etc.*) also cause a shift in the plane of reflection but, provided the gauge and platen to which the gauge is wrung are manufactured from the same material, these effects become comparatively small (a later report will present the results of experiments designed to investigate the magnitude of the error caused by effects other than that due to surface roughness).

The results of a literature search and theoretical study of the two effects can be found in an earlier internal report (Leach 1994a) and it is assumed that the reader is familiar with this or related work. The literature survey did not highlight a suitably accurate method for measuring the absolute magnitude of the length error caused by wringing a gauge to a platen. It is thought that the parameter that should be measured is the variability in the error when wringing is repeated. To do this a system has been designed that can exploit the use of existing and future high-accuracy phase-stepping interferometers.

Two instruments have been designed to measure the difference between optical and mechanical length measurements. This report presents a study of each instrument and discusses the prototype and final designs that will form part of the measurement service offered by NPL.

# 2 COUPLED PHASE-STEPPING INTERFEROMETER

## 2.1 OVERVIEW

If a gauge block is wrung to an optically polished dielectric flat, a small Fizeau cavity is formed between the surface of the flat and the effective optical plane of the gauge surface from which a light beam would be reflected (see figure 2.1). It can be proved, theoretically, that the effective optical plane of reflection is situated in the middle of the roughness profile of the gauge (O'Callaghan and Thwaite 1977). If a method is available to measure the phase change at reflection from the Fizeau cavity, the location of the effective optical plane of the gauge block can be calculated. To do this the flat-gauge combination is placed in one arm of a Twyman-Green interferometer and the phase from the Fizeau combination is compared to that from the free dielectric surface of the flat (Ishikawa and Bönsch *et. al.* 1992). It is easily shown that the phase change at reflection from a dielectric surface when used in transmission is zero, so this surface is used as a reference phase. The method of multiple-wavelength phase-stepping interferometry can then be used to extract the phase from the interference fringes from the gauge-flat combination. The resulting phase map can then be used to calculate the position of the effective optical plane of refelction.

Appendix A gives a full derivation of the phase change at reflection from a Fizeau cavity. Assuming normal incidence, the resulting expressions for the intensity reflection coefficient, $R$, and phase change at reflection, $\gamma$, are

$$R = 1 - \frac{(1-r_1^2)(1-r_2^2)}{1 + r_1^2 r_2^2 + 2r_1 r_2 \cos(\delta_2^+ - \Delta)} \tag{2.1}$$

$$\tan\gamma = \frac{(1-r_1^2) r_2 \sin(\delta_2^+ - \Delta)}{r_1(1+r_2^2) + r_2(1+r_1^2)\cos(\delta_2^+ - \Delta)} \tag{2.2}$$

where $r_1$ and $r_2$ are the amplitude reflection coefficients from the flat and gauge respectively, $\delta_2^+$ is the phase change at reflection at the air-gauge interface and $\Delta$ is the optical path-length of the air gap, given by

$$\Delta = \frac{4\pi d}{\lambda} \tag{2.3}$$

where $d$ is the geometrical length of the air gap (the roughness correction) and $\lambda$ is the incident wavelength. Rearranging equation (2.2) to make $d$ its subject gives

$$d = \frac{\lambda}{4\pi}\left[\delta_1^{+} - \tan^{-1}\left(\frac{c\tan\gamma}{a}\right) - \sin^{-1}\left(\frac{b\tan\gamma}{\sqrt{a^2 + c^2\tan^2\gamma}}\right)\right] \tag{2.4}$$

where the following substitutions have been made

$$\begin{aligned} a &= (1 - r_1^{\,2})r_2 \\ b &= (1 + r_2^{\,2})r_1 \, . \\ c &= (1 + r_1^{\,2})r_2 \end{aligned} \tag{2.5}$$

The amplitude reflection coefficients and phase changes at reflection from the two media in the flat-gauge Fizeau cavity can be found from the appropriate Fresnel equations and are given by

$$\begin{aligned} r_1 &= \frac{n_1 - 1}{n_1 + 1} \\ \delta_1^{+} &= 0 \\ r_2 &= \sqrt{\frac{(1 - n_2)^2 + k_2^{\,2}}{(1 + n_2)^2 + k_2^{\,2}}} \\ \delta_2^{+} &= \tan^{-1}\left(\frac{2k_2}{1 - n_2^{\,2} - k_2^{\,2}}\right) \end{aligned} \tag{2.6}$$

where $n_i$ is the refractive index of the $i^{\mathrm{th}}$ medium and $k_i$ is the absorption index. In the case of surface 1 being a dielectric optical flat $k_1 = 0$.

Figure 2.2 shows the relationship between $d$ and $\gamma$ with $n_1 = 1.4$, $n_2 = 2.4$, $k_2 = 3.4$ and $\lambda = 633$ nm. The factor $2\pi$ has been used to convert the phase into a fringe fraction that would be measured in a multiple-wavelength phase-stepping interferometer. In plotting figure 2.2 it was necessary to use a $2\pi$-unwrapping algorithm to remove discontinuities due to the tangent and arctangent functions present in equation (2.4).

It can be seen that, provided the optical constants are known, a measurement of fringe fraction resulting from the flat-gauge combination in a phase-stepping interferometer gives a measurement of the effective phase change at reflection caused by surface roughness or a roughness correction.

A potential problem with the system described above is the length error that is introduced due to wringing the gauge to the flat. Previous experimental results have shown that this error is smaller for a metal gauge wrung to an optically polished flat than for a metal gauge wrung to a more conventional metal platen (Rolt and Barrell 1927). This result would be expected due to the sub-nanometre surface finish of an optically polished flat. However, with the use of another optical flat it is possible to measure a roughness correction in such a way as to cancel the effects of wringing (see figure 2.3). Figure 2.3 (a) is the measurement that is described above and gives a measured length of

$$M_1 = w_1 + d \tag{2.7}$$

where $w_1$ is the length error introduced by wringing and $d$ is the roughness correction calculated from equation (2.4).

Figure 2.3 (b) is a conventional gauge block length measurement but with a flat as the platen and gives a measured length of

$$M_2 = L + w_2 + d \tag{2.8}$$

where $L$ is the measured length of the gauge and $w_2$ is the length error introduced by wringing. In figure 2.3 (c) flats have been wrung to both surfaces of the gauge in order to form a Fizeau cavity between the two dielectric surfaces. In this case part of the view of the bottom flat must be masked off to allow the top flat to act as a reference phase surface. In this case equation (2.4) reduces to

$$d = \frac{\lambda}{2\pi} \tan^{-1}\left( \frac{2n}{1+n^2} \cot \gamma \right) \tag{2.9}$$

where $n$ is the refractive index of the flats. The measured length is then given by

$$M_3 = L + w_1 + w_2. \tag{2.10}$$

Solving equations (2.7), (2.8) and (2.10) for $d$ gives

$$d = \frac{1}{2}(M_1 + M_2 - M_3) \tag{2.11}$$

which does not involve any of the effects due to wringing. Also, using this method the average effect of (glass-metal) wringing can be quantified as $M_2 - M_1 - M_3 = w_1 + w_2$.

It is important to note that this method for measuring a roughness correction will work for gauge blocks that are manufactured from any material. The total integrated scatter method described later will only work for metallic gauge blocks and platens. The crystal structure of the ceramic gauge block materials makes them almost perfect diffusers and the scalar scattering theory developed for a metallic surface does not apply. Ceramic materials are also subject to a high degree of translucency which significantly lowers the efficiency of an integrating sphere (Leach 1994b).

## 2.2 THE PROTOTYPE INSTRUMENT

A multiple-wavelength phase-stepping Twyman-Green interferometer - the Primary Length Bar Interferometer (PLBI) - has been developed at NPL that measures the length of long end standards (Lewis 1994a and 1994b). To test the theory behind the coupled interferometer it was decided that the existing phase-stepping interferometer would be used. This required some modifications to the optical mounting and the control and data processing software.

Two optical flats were manufactured from fused silica, both with front faces of flatness $\lambda/40$, back faces of $\lambda/8$ and with sub-nanometre surface finish ($\lambda$ = 633 nm) . The gauge is wrung to the $\lambda/40$ face and the $\lambda/8$ face is anti-reflection coated to avoid unwanted interference within the flat. Both flats were 50 mm in diameter and were 25 mm thick. The relatively large thickness ensures that the flats do not distort significantly due to the weight of a gauge and the forces due to wringing. Figure 2.4 shows the mounting configuration of the flat-gauge combination within the interferometer. The $\lambda/40$ flatness aluminium/$SiO_2$-coated Zerodur mirror deflects the beam vertically to allow the gauge-flat combination to be imaged in a position that causes the least distortion due the weight of the gauge.

Once the gauge-flat combination has been mounted and the optics have been aligned the resulting interferogram is imaged onto a CCD TV camera. The relative phase of the reference arm of the interferometer is moved in five discrete steps by a pre-determined amount and the intensity of the interferogram at each step is stored in the computer. The resulting five interferograms are processed using a phase-unwrapping algorithm from which the phase maps from the gauge-flat combination and the free surface of the flat can be compared. Finally the phase information is converted to information about the roughness correction using equation (2.4).

Experiments in the modified interferometer were carried out to investigate (a) whether fringes could be obtained from the flat-gauge combination, (b) if the difference in fringe contrast was acceptable when interference was obtained between the surface of the flat with the reference mirror compared to that between the flat-gauge combination and the reference mirror and (c) whether measurements of fringe fractions obtained using phase-stepping interferometry agree with the theoretical results displayed in figure (2.2). At this stage, the experiments were only designed to test the feasibility of the method and accurate results were not expected.

Fringes were easily obtained once the system was aligned. However, the difference between the fringe contrast off the flat and off the flat-gauge combination was high and could lead to significant modulation depth noise when the phase-stepping method is applied. This problem will have to be addressed at the next stage of the project (see next section). Measurements of fringe fractions gave results that are consistent with expected values for roughness corrections when they were processed using the equations determined in section (2.1). In conclusion these results proved that the method is indeed feasible.

## 2.3 DETAILED DESIGN OF THE FINAL INSTRUMENT

The final instrument will incorporate all of the desirable characteristics of the existing phase-stepping interferometer as well as some novel ideas. The size of the optical layout will be decreased to minimise effects due to the refractive index of the air and other sources of low-frequency phase noise. The dominant uncertainty source will be the error in the fringe fraction determination which mainly depends on the quality of gauge and flat surfaces. Higher quality flats will be produced from single-crystal quartz that have been cleaved along their optical axis and have a diameter of 60 mm. It is also possible to correct for the errors due to the flat and other optics in the system by simply operating the system without the gauge wrung to the flat. Theoretically, the result should be a phase map where every pixel represents zero phase. Any phase caused by the effects of non-ideal optics will give rise to a correction phase map that can be subtracted from phase maps produced during a measurement.

Fringe fraction samples will be used to check the accuracy and repeatability of the fringe fraction measurement. These are produced by depositing a thin metallic film in the shape of a gauge block onto a highly polished Zerodur substrate and then depositing another layer of the film over the existing film and the substrate. The height of the resulting step can be determined, to subnanometric accuracy, using calibrated mechanical stylus instruments at NPL (Franks 1993). The height of the step is less than $\lambda/2$ and hence the measurement of a fringe fraction gives the step height directly. Provided the top film is thick enough the effects due to the phase change at reflection do not need to be taken into account during a measurement as the two surfaces involved are optically and mechanically the same. This technique, therefore, gives a good measure of the effectiveness and repeatability of fringe fraction measurements.

A potential problem is the differential fringe-contrast, and equivalently the modulation depth, of the fringes from the free surface of the flat and that of the gauge-flat combination. This could lower the accuracy of the fringe fraction measurement. To match the contrasts, either the optical coatings of the reference mirror and the beam splitter will be redesigned, or a suitable optical filter will be employed.

Figure 2.5 shows a general assembly diagram for a final instrument. All the beam paths are much shorter than for the PLBI and the system uses less optical components. LS is a laser source that is coupled to a fibre optic delivery cable (FO). LS does not need to be frequency-stabilised and can be a relatively inexpensive He-Ne laser. FO is a monomode fibre that cuts down on speckle noise from LS and produces a diverging beam. The beam is steered into the main interferometer housing via mirror M1 and is collimated by a convex lens (CL). To fully illuminate the flat, that is used to produce the flat-gauge Fizeau system (FTG), the illuminating wavefront should have a diameter $\sqrt{2}d$ where $d$ is the diameter of the flat. The factor, $\sqrt{2}$, ensures filtering of high frequency components of the wavefront's beam spread function. The focal length of CL can be calculated from equation (2.12)

$$\mathrm{NA} = n \sin \theta \tag{2.12}$$

where NA is the numerical aperture of the monomode optical fibre (typically 0.17), $n$ is the refractive index of the surrounding medium ($n \approx 1$) and $\theta$ is half the divergence angle. Using trigonometry and equation (2.12) the focal length of CL is about 240 mm.

BS is a beam splitter that splits the beam into the reference and measurement components. The reference mirror, M3, is phase-stepped by an actuator system incorporating a high-precision single degree-of-freedom flexure stage with piezo-electric drives and capacitive feedback displacement control (PZT). The reference mirror assembly does not require two mirrors as in the PLBI. Mirror M2 steers the measurement beam onto FTG which is gimbal mounted to allow alignment with the remainder of the interferometer.

The reference and measurement wavefronts are re-combined at the beamsplitter, decollimated and imaged by lenses DL and IO and the interferogram is captured by a high definition CCD TV camera (CCD). The analogue interferogram from CCD is passed to a digital frame grabber, with a resolution of at least 640 × 480, and passed to a fast computer with at least 8 MBytes of RAM.

With some modifications, all of the above requirements can be achieved by placing FTG within the existing NPL/TESA gauge block interferometer (GBI). The modifications required will include the incorporation of phase-stepping techniques, some coating work to improve fringe contrast, a system to mount FTG and updates to the existing hardware and software systems. The option of modifying the GBI, as opposed to the development of a stand-alone system, will save on development time and cost, as well as opening up the option of technology transfer with existing GBIs around the globe.

Figure 2.6 shows the fringe pattern obtained by placing FTG within the GBI. The fringe contrast is superior to that obtained within the PLBI due to better matching of the reflectance from FTG and those from the reference mirror and beam-splitter.

# 3 TOTAL INTEGRATED SCATTER INSTRUMENT

## 3.1 OVERVIEW

It can be shown (see Appendix B for a full derivation) that the total integrated scatter (TIS), that is the ratio of the amount of light that is scattered by a sample, $I_d$, to the amount that would be reflected if the sample were perfectly smooth, $I_0$, is related to the RMS roughness of the surface, $\sigma$, by the following equation

$$\sigma = \frac{\lambda}{4\pi}\sqrt{\frac{I_d}{I_0}}. \tag{3.1}$$

In terms of the measurement of a gauge block wrung to a platen, the correction applied to the interferometrically measured length of a gauge is calculated by taking the difference between $\sigma$ measured for the platen and $\sigma$ for the gauge. The difference is then calibrated by comparison to the FTG method

## 3.2 EXPERIMENTAL SET-UP TO MEASURE TOTAL INTEGRATED SCATTER

To measure the diffuse component of the intensity in equation (3.1) it is necessary to integrate spatially the diffusely reflected radiation over the full $2\pi$ steradians into which it scatters. This can be achieved using an integrating sphere that takes the form of a hollow sphere which has its inside walls coated with a high diffuse reflectance material (Ulbricht 1900). The distribution of the scattered light is proportional to the power spectral density (PSD) function of the surface and any light reflected from the inner surface gives rise to a constant flux of electromagnetic power through any surface element of the sphere. The sphere has a number of ports to allow the radiation in and out, mounting of the sample to be irradiated and detectors to detect the integrated light. The work described in this report use an integrating sphere with the geometry shown schematically by figure 3.1.

A full description of the prototype instrument can be found elsewhere (Leach 1994b). The sample is held over the sample port using a suitable mount. The light enters the sphere through a 3 mm diameter input aperture and impinges on the sample at 8° incidence. The specular component of the reflected intensity exits the sphere through a 3 mm diameter output aperture and its intensity is measured. The scattered component of the intensity is spatially integrated by the sphere and measured at the detection port. It is important that the detection port is baffled from the sample port to avoid scattered radiation being detected before it has been integrated spatially. The baffle must also be coated with the same material as the walls of the sphere.

The integrating sphere used (L.O.T. - Oriel 70451) had a diameter of 152 mm and was equipped with three 38 mm diameter ports and an inside coating of barium sulphate (at $\lambda$ = 672 nm the diffuse reflectance is greater than 98%). A disc was inserted into the input port which contained the input and output apertures. A mount for the sample, that attaches to the sample port using a specially designed coupling ring, allows a 5 × 5 mm area of the sample to be illuminated. The remaining parts of the mount and the inside face of the input/output aperture disc, which take up the area of the ports, were painted with barium sulphate to match the reflectance of the walls.

The optical layout is shown in figure 3.2. The source is a 672 nm, 1 mW laser diode (LS). The laser beam passes through a 4× beam expander and collimator (BE&C), is linearly polarised and passes through a quarter wave-plate (P&$\lambda$/4) where it is circular polarised to avoid differential optical effects for the *s*- and *p*-polarisation states.

The laser beam passes through a 3 mm diameter aperture (SF) to reduce the beam diameter, through a 305 mm focal length lens (FL), which focuses it onto the output aperture, through the input aperture into the integrating sphere (IS) and reflects off the surface of the sample (S). The specularly reflected light exits the sphere through the output aperture and is detected by PD1. It is important to align the system such that all the specularly reflected light exits through the output aperture. The diffuse component of the intensity is detected by another photodetector (PD2) that is suitably coupled to the detector port of the sphere.

Two photodetectors are required to measure the incident, diffuse and specular components of the intensity. To avoid the $1/f$, or flicker noise, the principles of phase sensitive detection and lock-in amplification were employed. The laser diode source was modulated at 498 Hz by use of a mechanical light chopper. The effect of the modulation is to centre the signal at the fast modulation frequency rather than at dc, in order to get away from $1/f$ noise. This also suppresses all noise sources (such as room lights) which are not oscillating at the modulation frequency. Phase sensitive detection is then used to demodulate and bandpass filter the signal.

## 3.3 MEASUREMENT PROCEDURE

The total integrated scatter is defined as the ratio of the diffusely reflected intensity, $I_d$, to the total reflected intensity, $I_0$. As pointed out in Appendix B it is never possible to measure $I_0$. However, provided the slightly rough surface assumption applies, $I_0$ can be assumed to be equal to the specularly reflected intensity, $I_s$. In this case the TIS will also be equal to the ratio of the diffuse and specular reflectance values. Another important practical point when comparing intensities, arises due to the different optical and electronic set-ups used to measure such intensities. Each detector will have an associated efficiency factor which is a function of its delivery optics and image geometry. In practice equation (3.1) should be written

$$\sigma = \frac{\lambda}{4\pi}\sqrt{\frac{I_d \eta_d}{I_0 \eta_0}} \tag{3.2}$$

where $\eta_d$ and $\eta_0$ are the efficiency factors of the two detectors. It is possible to avoid this problem by using a sample with 'known' diffuse reflectance (Detrio and Miner 1985). In the following calculation the subscripts *s*, *d*, *i* and *ref* represent specular, diffuse, incident and reference, respectively. The actual specular reflectance that can be measured is given by

$$R_s = \frac{P_s}{P_i} \tag{3.3a}$$

and the diffuse reflectance is given by

$$R_d = \frac{P_d}{P_i} \tag{3.3b}$$

where $P_j$ are the respective radiant powers. The detection process employed gives a voltage reading which is proportional to the radiant power thus

$$V_j = P_j \zeta \eta_j \tag{3.4}$$

where $V_j$ is the signal measured by the $j^{\text{th}}$ detector, $\zeta$ is the response of the detector and its amplification electronics (V W$^{-1}$) and $\eta_j$ is its efficiency. Now the TIS is given by the ratio of the diffuse and specular radiant powers which is also equal to the ratio of the diffuse and specular reflectance, so from equation (3.3b) and (3.4)

$$\frac{P_d}{P_s} = \frac{R_d}{R_s} = \frac{V_d/(\zeta\eta_d)}{R_s P_i}. \tag{3.5}$$

To avoid using the efficiency factors for different detectors' delivery optics, a diffuse reference scatterer is used which has a voltage measured by the diffuse detector of

$$V_{ref} = P_i R_{ref} \zeta \eta_d \tag{3.6}$$

so that

$$\frac{R_d}{R_s} = \frac{V_d}{\zeta\eta_d}\frac{\zeta\eta_d}{V_{ref}}\frac{R_{ref}}{R_s}. \tag{3.7}$$

Finally, combining equations (3.1) and (3.7) gives

$$\sigma = \frac{\lambda}{4\pi}\sqrt{\frac{V_d}{V_{ref}}\frac{R_{ref}}{R_s}}. \qquad (3.8)$$

Equation (3.8) shows that it is not necessary to calibrate the integrating sphere's optical characteristics as any associated linear calibration constants will cancel due to the ratio $V_d/V_{ref}$. Therefore, a reference diffuse reflector was manufactured and calibrated by the Spectrophotometry and Colorimetry Section in the Division of Quantum Metrology at NPL. The active surface of the reflector was made from a white ceramic tile material with the same dimensions as the working face of a gauge block. It was calibrated using an Instrumental Colour System Micro Match spectrophotometer by comparison to an NPL master. The calibration was carried out over a wide spectral bandwidth (380 - 780 nm in 5 nm steps) and the total and diffuse reflectance were measured.

When measuring a gauge or platen the following procedure is carried out:

(1) Place the reference reflector at the sample port.
(2) Measure the incident voltage by placing PD1 at a suitable position in the incident beam ($V_i$).
(3) Measure the voltage on PD2 ($V_{ref}$).
(4) Place the gauge in the sample port.
(5) Measure the specularly reflected voltage by placing PD1 in a suitable position in the specularly reflected beam ($V_s$).
(6) Measure the voltage on PD2 ($V_d$).
(7) Repeat steps (1), (2) and (3) to check for drift in the laser beam intensity.
(8) If the laser intensity has not drifted, calculate $\sigma$ from equation (3.8).

The above procedure is carried out for both the gauge and platen and the roughness correction is the difference between the two measured values of $\sigma$.

## 3.4 DETAILED DESIGN OF THE FINAL INSTRUMENT

The experimental results with the prototype instrument illustrated a number of points that will be addressed in the final design. The optics will be more rigorously mounted and easier to align. The modulation of the source will be accomplished by modulating the injection current of the laser diode. The design of the input/output aperture port and the systems used to couple the detector and the sample to their respective ports will be re-designed, in conjunction with the NPL Engineering Services, to raise the efficiency of the integrating sphere. The photodetectors will be calibrated in the Division of Quantum Metrology at NPL for linearity and to match their responses. The size of the output aperture will be decreased to minimise the amount of diffuse light that is lost around the direction of specular reflection (in theory the minimum size of the aperture, dictated by the size of the Airy disk, for a 300 mm focal length lens and a 3 mm diameter input aperture is 100 μm).

For the prototype instrument, two separate phase sensitive detectors (PSDs) were used to read the voltages from the photodetectors (the incident and specular components were detected using the same detector). The final system will incorporate a single, purpose-built PSD and use multiplexing to read the three voltages. These systems plus a high-accuracy, calibrated digital voltmeter (DVM) will be housed in an electronics rack incorporating an IEEE-488 interface (see figure 3.3).

The final system will have a spatial filtering system as part of the delivery optics. This consists of a microscope objective system that focuses onto a 10 μm pinhole. The instrument will be designed in such a way as to adjoin to the interferometer cabinet of the NPL gauge block interferometer. The whole system will be contained in a suitable box that minimises the amount of stray light entering the system but allows the sample to be placed over the sample port.

Once the final instrument has been produced, a comparison will be made with the TIS instrument at Physikalisch-Technische Bundesanstalt (PTB) for a chosen sample of gauges and platens from a reference set. Comparisons will also be made with the results obtained using the coupled phase-stepping interferometer, the existing NPL stack method and a method being developed at NPL that uses the well-characterised properties of thin-films.

# 4 AN INSTRUMENT TO MEASURE THE VARIABILITY IN THE LENGTH ERROR INTRODUCED BY WRINGING

## 4.1 INTRODUCTION

The process of wringing is used to bring a gauge into close contact with the platen. This report will not discuss the theory or practice of wringing but the details can be found in an earlier review (Leach 1994a). No methods that were sufficiently accurate enough for measuring the absolute contact error due to wringing were identified in the literature. However, it is the variability in this error when wringing is repeated that is of most importance. In section 2 a method was identified for measuring the contact error due to wringing a highly-polished optical flat to a gauge block. The physics and literature suggest that this gives rise to an error that is much more repeatable and much smaller in magnitude than that obtained when a gauge is wrung to a platen surface.

The next section describes a method for measuring the variability in the contact error due to wringing that utilises existing and future high-accuracy phase-stepping interferometers.

## 4.2 THE PROTOTYPE INSTRUMENT TO MEASURE THE CONTACT ERROR DUE TO WRINGING

Once again the PLBI will be used to carry out wringing repeatability experiments. A reference platen has been designed that will be mounted in place of the flat-gauge Fizeau combination described in section 2. Figure 5.1 shows a general assembly diagram for the reference platen and its associated mount. The platen surface is flat to 12 nm and has an average surface roughness of about 10 nm. It has been designed to relocate in a semi-kinematic support. A nylon mask has been designed that will ensure that a gauge can be repeatedly wrung in approximately the same position on the platen.

The work involved wringing a gauge to the reference platen and measuring its central length in the normal manner. The gauge is then taken off the platen and re-wrung. Sufficient time is allowed for the platen and gauge to reach thermal equilibrium and the central length measurement is repeated. Measurements using the PLBI are carried out in a highly stable environmental chamber which is itself contained in a temperature-controlled room. The whole process is repeated a number of times. All systematic components of the uncertainty in the length measurement will be the same for each repeated measurement. However, there will still be random components of uncertainty which will be dominated by the accuracy of the fringe-fraction calculation (± 1 nm at one standard deviation). The literature quotes values for the variability of the contact error due to wringing of as much as ± 20 nm.

This magnitude of variation would clearly be seen by such experiments. The experiments would also indicate whether there is any secular change in length upon repeated wringing and this could be varified by experiments that are being carried out as part of this project to characterise a reference set of gauge blocks and platens.

## 5 DISCUSSION

Three instruments have been developed that will reduce the measurement uncertainties offered by NPL in the field of gauge block measurement. This reduction is necessary, and will continue to be required in the future, by the precision engineering industries and by users of high-accuracy co-ordinate measuring machines. The instruments measure a correction for the phase change at reflection from the surfaces of the gauge and platen and the variability in the contact error due to wringing. The interferometric method of measuring a phase correction is the most accurate method available. However, the total integrated scatter method will have the benefits of speed and ease of use. Both methods achieve the target uncertainty of ± 6 nm. The next stage of the project was to construct the final-stage instruments and these results will be described in two later reports

## REFERENCES


Allardyce, K. J., George, N. Diffraction analysis of rough reflective surfaces. *Appl. Opt.*, 1987, **26**, 2364-2375.

Born, M., Wolf, E. *Principles of optics.* Pergamon Press, Oxford, 1975 (6th edition).

Church, E. L., Zavada, J. M. Residual surface roughness of diamond turned optics. *Appl. Opt.*, 1975, **14**, 1788-

Davies, H. Reflection of electromagnetic waves from a rough surface. *Proc. Inst. Elec. Engrs.*, 1954, **101**, 209-214.

Detrio, J. A., Miner, S. M. Standardised total integrated scatter measurements of optical surfaces. *Opt. Eng.*, 1985, **24**, 419-422.

Elson, J. M., Rahn, J. P., Bennett, J. M. Relationship of total integrated scattering from multilayer-coated optics to angle of incidence, polarisation, correlation length and roughness cross-correlation properties. *Appl. Opt.*, 1983, **22**, 3207-3219.

Franks, A. Progress towards traceable nanometric surface metrology. *Nanotechnology*, 1993, **4**, 200-205.

Ishikawa, S., Bönsch, G., Böhme, H. Phase-shifting interferometry with a coupled interferometer: Application to optical roughness of gauge blocks. *Optik*, 1992, **91**, 103-108.

Leach, R. K., Measurement of the phase change on reflection and the contact error due to wringing. *NPL DMOM Report*, 1994a.

Leach, R. K. *Development of an instrument to measure phase change at reflection.* MSc Thesis, Brunel University, 1994b.

Lewis, A. J. *Absolute length measurement using multiple-wavelength phase-stepping interferometry.* PhD Thesis, Imperial College of Science, Technology and Medicine, 1994a.

Lewis, A. J. Measurement of length, surface form and thermal expansion coefficient of length bars up to 1.5 m using multiple-wavelength phase-stepping interferometry. *Meas. Sci. Technol.*, 1994b, **5**, 694-703.

Pugh, D. J., Jackson, K. Automatic gauge block measurement using multiple wavelength interferometry. *Proc. SPIE*, 1986, **656**, 244-250.

O'Callaghan, M., Thwaite, E. G. The expectation of the electromagnetic field scattered from a random rough surface. *National Measurement Laboratory Report*, 1977, **NMLR 9**.

Ogilvy, J. A. *Theory of wave scattering from random rough surfaces.* Adam Hilger, Bristol, 1991.

Rolt, F. H., Barrell, H. Contact of flat surfaces. *Proc. Roy. Soc.*, 1927, **A116**, 401-425.

Ulbricht, R. von Die Bestimmung der mittleren räumlichen Lichtintensität durch nur eine Messung. *Electrotechnische Zeitschrift*, 1900, **29**, 595-601.

**APPENDIX A** - CALCULATION OF THE PHASE CHANGE AT REFLECTION FROM A FIZEAU INTERFEROMETER

Consider the Fizeau interferometer shown in figure A.1 in which two plates are separated by an air gap of geometrical length $d$. $r_1$ and $r_2$ are the amplitude reflection coefficients of the two plates, $\delta_1^+$ and $\delta_2^+$ are the phase changes at reflection in the positive $x$-direction (medium-air interface), $\delta_1^-$ is the phase change at reflection in the negative $x$-direction (air-medium interface), $t$ is the transmission coefficient of medium 1 (assumed equal in both directions) and $\theta$ is the angle of incidence.

The amplitude that is reflected from the whole system is calculated by summing the complex amplitudes of the multiple reflected beams and is given by

$$A = re^{i\gamma} = r_1 e^{i\delta_1^+} + t^2 r_2 e^{i(\delta_2^+ - \Delta)} + t^2 r_1 r_2^2 e^{i(2\delta_2^+ - 2\Delta - \delta_1^-)} + \ldots \tag{a.1}$$

where $r$ is the amplitude reflection coefficient and $\gamma$ is the phase change at reflection for, the total system and $\Delta$ is the 'optical length' of the Fizeau cavity, given by

$$\Delta = \frac{4\pi n d}{\lambda}\cos\theta \tag{a.2}$$

where $n$ is the refractive index of the air gap, henceforth assumed equal to unity. With the exception of the first beam, each successive beam forms a geometrical progression with the factor $r_1 r_2 e^{i(\delta_2^+ - \Delta)}$. The sum to infinity of all the terms in equation (a.1) gives

$$re^{i\gamma} = r_1 e^{i\delta_1^+} + \frac{t^2 r_2 e^{i(\delta_2^+ - \Delta)}}{1 - r_1 r_2 e^{i(\delta_2^+ - \Delta - \delta_1^-)}}. \tag{a.3}$$

In the case of medium 1 being a dielectric, $\delta_1^+ = 0$, $\delta_1^- = \pi$ and $t^2 = 1 - r_1^2$. Equation (a.3) then becomes

$$\begin{aligned} re^{i\gamma} &= r_1 + \frac{(1 - r_1^2) r_2 e^{i(\delta_2^+ - \Delta)}}{1 - r_1 r_2 e^{i(\delta_2^+ - \Delta - \pi)}} \\ &= \frac{r_1 + r_2 e^{i(\delta_2^+ - \Delta)}}{1 + r_1 r_2 e^{i(\delta_2^+ - \Delta)}} \end{aligned} \tag{a.4}$$

To calculate $\gamma$ the numerator and denominator of equation (a.4) are multiplied by the complex conjugate of the denominator and the real and imaginary parts of the resulting expression are resolved. After some simple algebra the following expressions are obtained

$$R = r^2 = 1 - \frac{(1 - r_1^{\,2})(1 - r_2^{\,2})}{1 + r_1^{\,2} r_2^{\,2} + 2 r_1 r_2 \cos(\delta_2^{\,+} - \Delta)} \tag{a.5}$$

$$\tan\gamma = \frac{(1 - r_1^{\,2}) r_2 \sin(\delta_2^{\,+} - \Delta)}{r_1(1 + r_2^{\,2}) + r_2(1 + r_1^{\,2})\cos(\delta_2^{\,+} - \Delta)} \tag{a.6}$$

where $R$ is the intensity reflection coefficient.

## **APPENDIX B** - THEORY OF TOTAL INTEGRATED SCATTER

Scattering from a surface is caused by surface roughness, variations in the optical constants of the surface, subsurface damage, particulates, scratches and other defects which are large compared to the wavelength of the incident radiation. It is not yet analytically possible to take into account all the physical processes which occur in the phenomena of reflection, but firm knowledge may be gained by using numerical techniques or by using realistic simplifying assumptions about the nature of the problem. Much of the work stems from the fields of either acoustic or long wavelength electromagnetic wave reflection from the surface of the sea, in which case a common simplifying assumption is that the wavelength of the incident wave is much larger than the roughness of the surface. This is known as the 'slightly rough surface' assumption. In the case of gauge block interferometry the wavelength of the incident radiation is commonly 633 nm and the RMS surface roughness of a high quality gauge block surface is in the order of 10 nm. It is not clear that the slightly rough surface assumption is valid for this situation. However, the following calculation relies heavily on the slightly rough surface assumption in the hope that any insights gained will outweigh the inaccuracy of the physics. To begin with, five more assumptions are necessary:

(i) The surface is not so precipitous that some parts of it are hidden or shielded from the incident beam. In the case of quasi-normal incidence this is a very fair assumption.

(ii) The surface has infinite conductivity, *i.e.* it is a perfect conductor, and, therefore, if it were perfectly smooth there would be no scatter. In the case of a steel surface being irradiated with optical frequencies this assumption is somewhat dubious. Also, the surface plasma excitations caused by the incident radiation are the same as those for a perfectly smooth surface, *i.e.* there is no roughness-induced drop in the reflectance of the surface due to surface-plasmon-coupling (Church and Zavada 1975).

(iii) The distribution of surface heights and the autocorrelation function are Gaussian about the mean. This is a good assumption if many different processes have been involved in manufacturing the surface (Central Limit theorem). Elson and Rahn *et. al.* (1983) have proved that, whilst this assumption is mathematically convenient, it is not necessary.

(iv) The surface roughness is isotropic, *i.e.* the surface has no lay. This is not strictly true for a ground and lapped surface. It is, however, not such a daunting task to extend the calculation to an anisotropic surface. In this case the mean square slope, $q^2$ in equation (b.19), would be replaced by the product of two mean slopes representing the $x$ and $y$ directions.

(v) The reflectance of the surface is the same when the surface is rough as when it is smooth. This is a reasonable assumption when the surface is illuminated with a beam whose width is large compared to the roughness parameters of the surface.

The calculation below essentially follows that due to Davies (1954) and uses scalar scattering theory (the same result is obtained using Kirchoff theory). Some adjustments have been made to lead towards results useful in the application of total integrated scatter (Davies' application was for radar in a marine environment).

Consider a plane wave that is incident on a rectangular surface with the $x$- and $y$-axes in the plane of the surface and the $z$-axis normal to the surface. The surface has dimensions $a\times b$. From diffraction theory the field of the reflected wave is given by the Fresnel-Kirchoff formula (Born and Wolf 1975)

$$\begin{aligned}\psi &= \frac{\psi_0}{2\lambda r}\iint_{\text{surface}} ds(\cos\phi_1+\cos\theta) \\ &\quad\times\exp\left\{\frac{2\pi i}{\lambda}\left[x(\sin\phi_1\cos\phi_2-\sin\theta)+y\sin\phi_2\sin\phi_2+z(\cos\phi_1+\cos\theta)\right]\right\} \\ &= \frac{\psi_0}{2\lambda r}\int_{-a/2}^{a/2}dx\int_{-b/2}^{b/2}dy f[x,y,z(x,y)]\end{aligned} \tag{b.1}$$

where $ds = dxdy$, $\lambda$ is the wavelength of the incident beam, $r$ is the perpendicular distance from the surface, $\theta$ is the angle of incidence, $\phi_1$ and $\phi_2$ are the reflection and azimuth scattering angles respectively (see figure B.1), $\psi_0$ is the incident electric field strength and $z = z(x,y)$ is a continuous random function representing the distribution of the surface heights.

If the surface were perfectly smooth, *i.e.* $z = 0$ then

$$\psi = \frac{\psi_0}{2\lambda r}(\cos\phi_1+\cos\theta)\frac{\sin\left[\frac{\pi a}{\lambda}(\sin\phi_1\cos\phi_2-\sin\theta)\right]}{\frac{\pi}{\lambda}(\sin\phi_1\cos\phi_2-\sin\theta)}\frac{\sin\left(\frac{\pi b}{\lambda}\sin\phi_1\sin\theta\right)}{\frac{\pi}{\lambda}\sin\phi_1\sin\theta}. \tag{b.2}$$

Equation (b.2) is the normal diffraction pattern with a central maximum in the direction of specular reflection. It can be shown, with the aid of l'Hôpital's limit theorem, that at normal incidence, when $\theta = \phi_1 = 0$, the field equation reduces to the simple form

$$\psi = \frac{\psi_0}{\lambda r}ab \tag{b.3}$$

which is a purely specular beam in the opposite direction to incidence. The mean value of the reflection field can be split into two components: a coherent, specular field $\langle \psi \rangle$ and an incoherent, diffuse or deviation field $\psi - \langle \psi \rangle$. At normal incidence

$$\langle \psi \rangle = \frac{\psi_0}{\lambda r} \iint \left\langle \exp\left[\frac{4\pi i z}{\lambda}\right] \right\rangle dxdy. \tag{b.4}$$

Assuming the distribution of heights is Gaussian the corresponding probability density function is

$$p(z) = \frac{1}{\sigma\sqrt{2\pi}} \exp\left(-\frac{z^2}{2\sigma^2}\right) \tag{b.5}$$

where $\sigma$ is the RMS roughness of the surface. From the probability density function it follows that

$$\left\langle \exp\left[\frac{4\pi i z}{\lambda}\right] \right\rangle = \exp\left[-\frac{8\pi^2\sigma^2}{\lambda^2}\right] \tag{b.6}$$

and that

$$\langle \psi \rangle = \frac{\psi_0}{\lambda r} ab \exp\left(-\frac{8\pi^2\sigma^2}{\lambda^2}\right). \tag{b.7}$$

This is the usual specular reflection pattern, at normal incidence, modified by a factor in $\sigma/\lambda$. The deviation field is given by

$$\psi - \langle \psi \rangle = \frac{\psi_0}{\lambda r} \iint \left\{ \exp\left[\frac{4\pi i z}{\lambda}\right] - \exp\left[-\frac{8\pi^2\sigma^2}{\lambda^2}\right] \right\} dxdy. \tag{b.8}$$

Applying the slightly rough surface assumption, *i.e.* $z/\lambda << 1$ and $\sigma/\lambda << 1$, only first order powers need to be considered in equation (b.8) and

$$\psi - \langle \psi \rangle = \frac{4\pi i \psi_0}{\lambda^2 r} \iint z(x,y) dxdy. \tag{b.9}$$

The intensity averaged over the full ensemble of reflectors is given by

$$\left| \psi - \langle \psi \rangle \right|^2 = \frac{16\psi_0{}^2\pi^2}{\lambda^4 r^2} \iint z(x,y) dxdy \iint z(x',y') dx'dy' \tag{b.10}$$

where $x' = x$ plus a spatial shift in the $x$ direction. The average deviation intensity is given by

$$\left\langle \left|\psi - \langle\psi\rangle\right|^2 \right\rangle = \frac{16\psi_0^{\ 2}\pi^2}{\lambda^4 r} \int\int\int\int dxdydx'dy' \langle z(x,y)z(x',y')\rangle \qquad \text{(b.11)}$$

where $\langle z(x,y)z(x',y')\rangle/\sigma^2$ is the two dimensional autocorrelation function of the surface heights (Ogilvy 1991). Using the assumption that the statistics of the surface follow a Gaussian distribution we have

$$\langle z(x,y)z(x',y')\rangle = \sigma^2 \exp\left\{-\frac{1}{\lambda_0^{\ 2}}\left[(x-x')^2 + (y-y')^2\right]\right\} \qquad \text{(b.12)}$$

where $\lambda_0$ is the autocorrelation length, this being the distance over which the autocorrelation function falls off by 1/e. Let $x' = x + X$ and $y' = y + Y$ and we have

$$\left\langle \left|\psi - \langle\psi\rangle\right|^2 \right\rangle = \frac{16\pi^2\psi_0^{\ 2}}{\lambda^4 r^2} \int\int\int\int dxdydXdY\sigma^2 \exp\left[-\frac{1}{\lambda_0^{\ 2}}(X^2+Y^2)\right]. \qquad \text{(b.13)}$$

If $a$ and $b$ are a lot bigger than $\lambda_0$ the domains of integration are given by

$$-\infty \le X,Y \le \infty$$
$$-a/2 \le x \le a/2$$
$$-b/2 \le y \le y/2.$$

The part of equation (b.13) which is a Gaussian integral solves to give

$$\int_{-\infty}^{\infty}\int_{-\infty}^{\infty} dXdY \exp\left[-\frac{1}{\lambda_0^{\ 2}}(X^2+Y^2)\right] = \lambda_0^{\ 2}\pi \qquad \text{(b.14)}$$

and hence equation (b.13) reduces to

$$\left\langle \left|\psi - \langle\psi\rangle\right|^2 \right\rangle = \frac{16\pi^3\psi_0^{\ 2}\lambda_0^{\ 2}}{\lambda^4 r^2} ab. \qquad \text{(b.15)}$$

Equation (b.15) describes the scattered or diffuse component of the total average intensity of the reflected beam at normal incidence. The total average reflected intensity is thus given by the sum of the specular and the diffuse beams, *i.e.*

$$\left\langle |\psi|^2 \right\rangle = \langle\psi\rangle^2 + \left\langle \left|\psi - \langle\psi\rangle\right|^2 \right\rangle. \qquad \text{(b.16)}$$

Using equations (b.8) and (b.15) we have

$$\langle|\psi|^2\rangle = \frac{\psi_0{}^2}{\lambda^2 r^2} a^2 b^2 \exp\left(-\frac{16\pi^2\sigma^2}{\lambda^2}\right) + \frac{16\pi^3 \psi_0{}^2 \lambda_0{}^2}{\lambda^4 r^2} ab. \tag{b.17}$$

Considering the average intensity per unit area, equation (b.17) becomes

$$\langle|\psi|^2\rangle = \frac{\psi_0{}^2}{\lambda^2 r^2} \exp\left(-\frac{16\pi^2\sigma^2}{\lambda^2}\right) + \frac{16\pi^3 \psi_0{}^2 \lambda_0{}^2}{\lambda^4 r^2}. \tag{b.18}$$

The diffuse component of equation (b.18) can be written

$$\langle|\psi - \langle\psi\rangle|^2\rangle = \frac{32\pi^3 \psi_0{}^2 \sigma^2}{q^2 \lambda^4 r^2} \tag{b.19}$$

where $q$ is the RMS slope of the surface and is given by (Bennett and Porteus 1961)

$$q = \frac{\sqrt{2}\sigma}{\lambda_0}. \tag{b.20}$$

It can be seen that the diffuse component, which is dependent on $\lambda^{-4}$, makes a negligible contribution to the overall reflected intensity as $\lambda \to \infty$ or $\lambda >> \sigma$ (the slightly rough surface assumption). Assuming the reflected intensity from a perfectly flat surface, $I_0 = \psi_0{}^2/\lambda^2 r^2$ and ignoring the diffuse component, the total reflected intensity, $I$, from the rough surface is given by

$$I = I_0 \exp\left[-\frac{(4\pi\sigma)^2}{\lambda^2}\right]. \tag{b.21}$$

Provided $I/I_0 \approx 1$, equation (b.21) expands to give

$$\sigma = \frac{\lambda\sqrt{I_0 - I}}{4\pi\sqrt{I_0}}. \tag{b.22}$$

Now $I_0 - I$ is simply the diffuse component of the intensity, $I_d$ and, therefore equation (b.22) becomes

$$\sigma = \frac{\lambda}{4\pi}\sqrt{\frac{I_d}{I_0}}. \tag{b.23}$$

$I_d/I_0$ is known as the total integrated scatter (TIS). It must always be remembered that $I_0$ is not the intensity of the specularly reflected beam, $I_s$, and can, in reality, never be measured. However, if the slightly rough surface assumption applies, $I_0$ will be approximately equal to $I_s + I_d$.

To understand the physics of the slightly rough surface assumption it is helpful to consider the surface as a sinusoidal grating. When the amplitude of the grating, equivalent to $\sigma$, is small compared to $\lambda$, the reflection pattern will be entirely determined by diffraction effects; the specular component of the beam being the zeroth diffraction order. As $\lambda$ approaches the magnitude of the amplitude of the grating, the reflection pattern will be determined by both the amplitude and the slope of the grating. Finally, as $\lambda$ becomes smaller than the amplitude the reflection pattern will be determined entirely from the slope of the grating and could be described using the laws of geometrical optics. A thorough investigation of diffraction effects at rough reflective surfaces is given elsewhere (Allardyce and George 1987). It is expected, when realising equation (b.23) using TIS instrumentation and with $\lambda \sim 10\sigma$, that both the heights and slopes of the surface will be significant. Equation (b.18) would then be the best description of the reflected intensity. This is the expected situation in the field of gauge block interferometry. It is, therefore, expected that when measuring $\sigma$ using TIS methods the result will be more akin to a correction for the optical phase change at reflection due to surface roughness than simply the value of $\sigma$ which would be measured using a surface profilometer such as a mechanical stylus method.

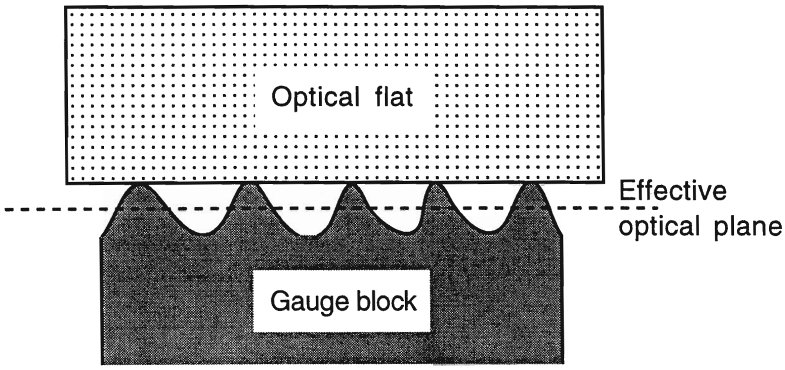


**Figure 2.1** Effective optical plane of reflection when a gauge block is wrung to an optically polished flat

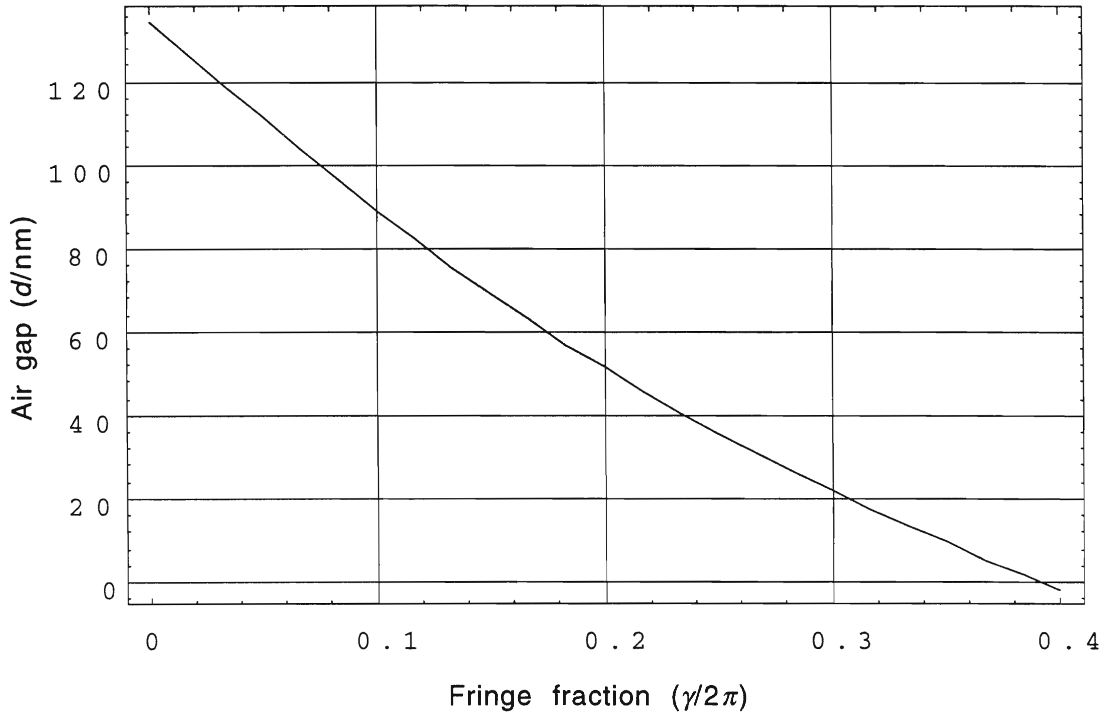


**Figure 2.2** Geometrical length of air gap against fringe fraction for a Fizeau interferometer

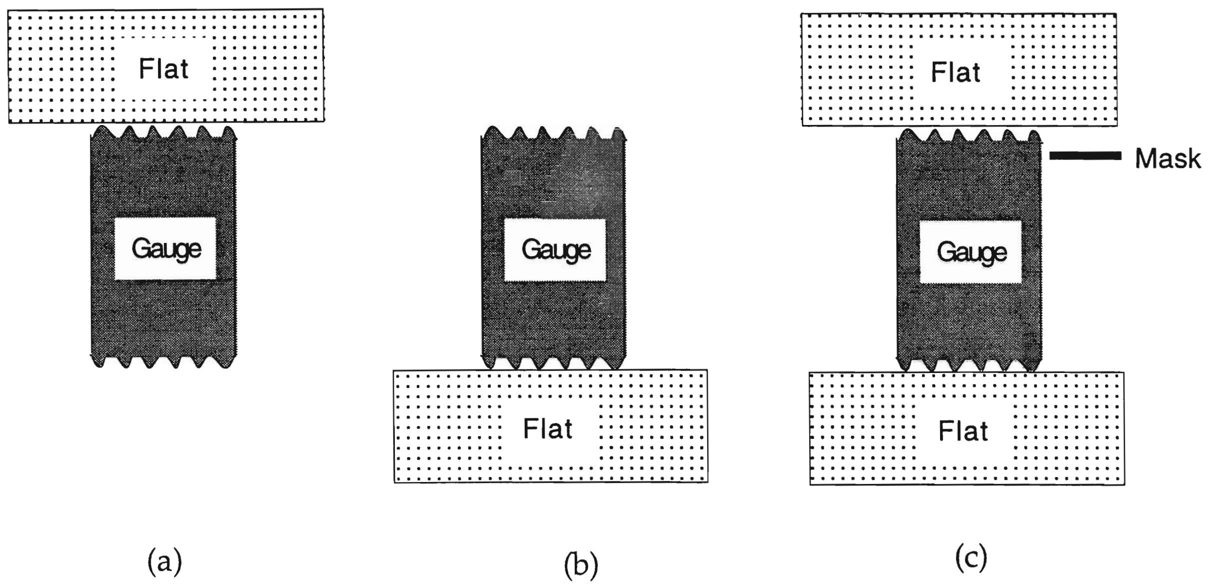


**Figure 2.3** Experimental method used to measure a roughness correction independent of the length error introduced by wringing (the incident light travels from the top to the bottom of the diagram)

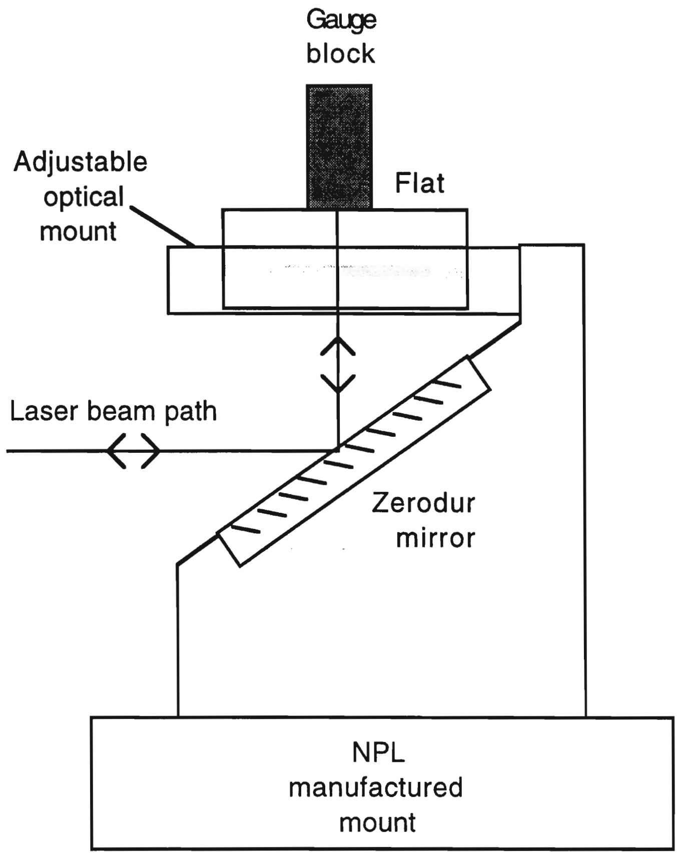


**Figure 2.4** Mounting configuration of the flat-gauge Fizeau combination within the Primary Length Bar Interferometer

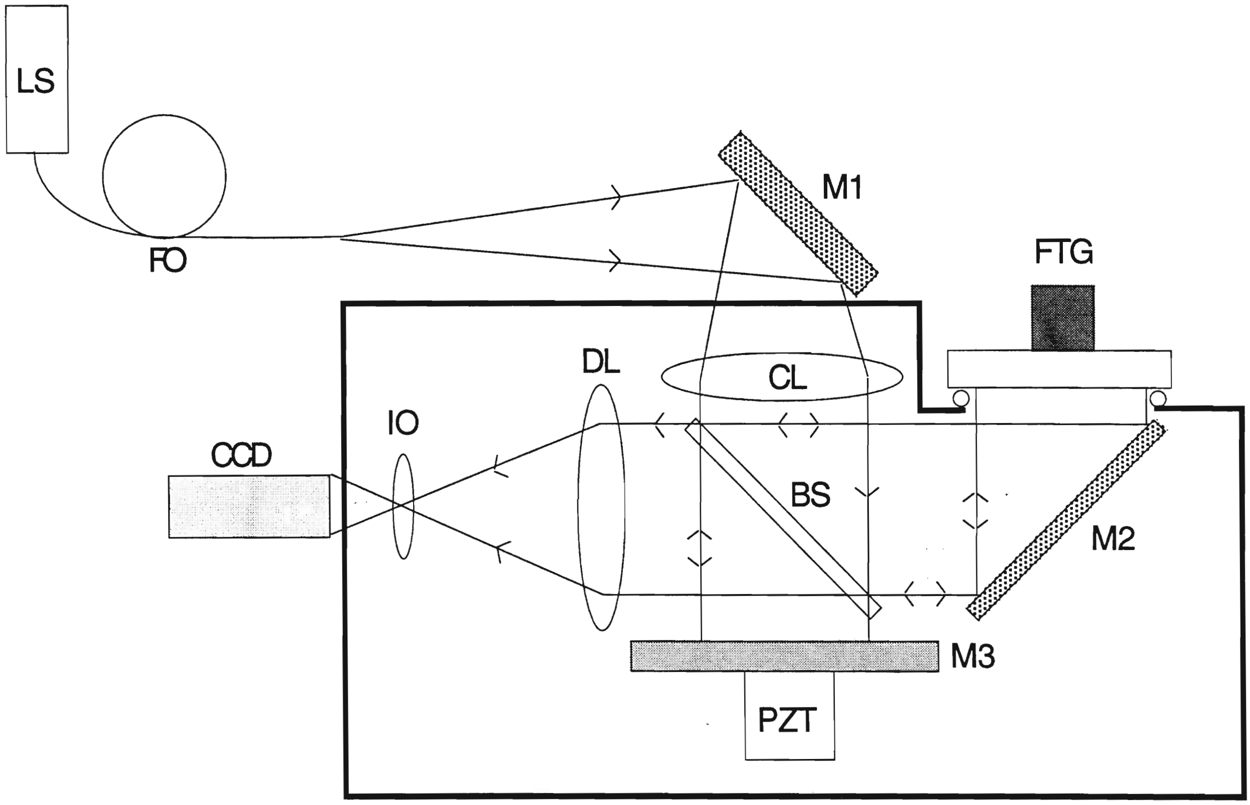


**Figure 2.5** General assemble diagram of the coupled interferometer (annotations are described in the accompanying text)

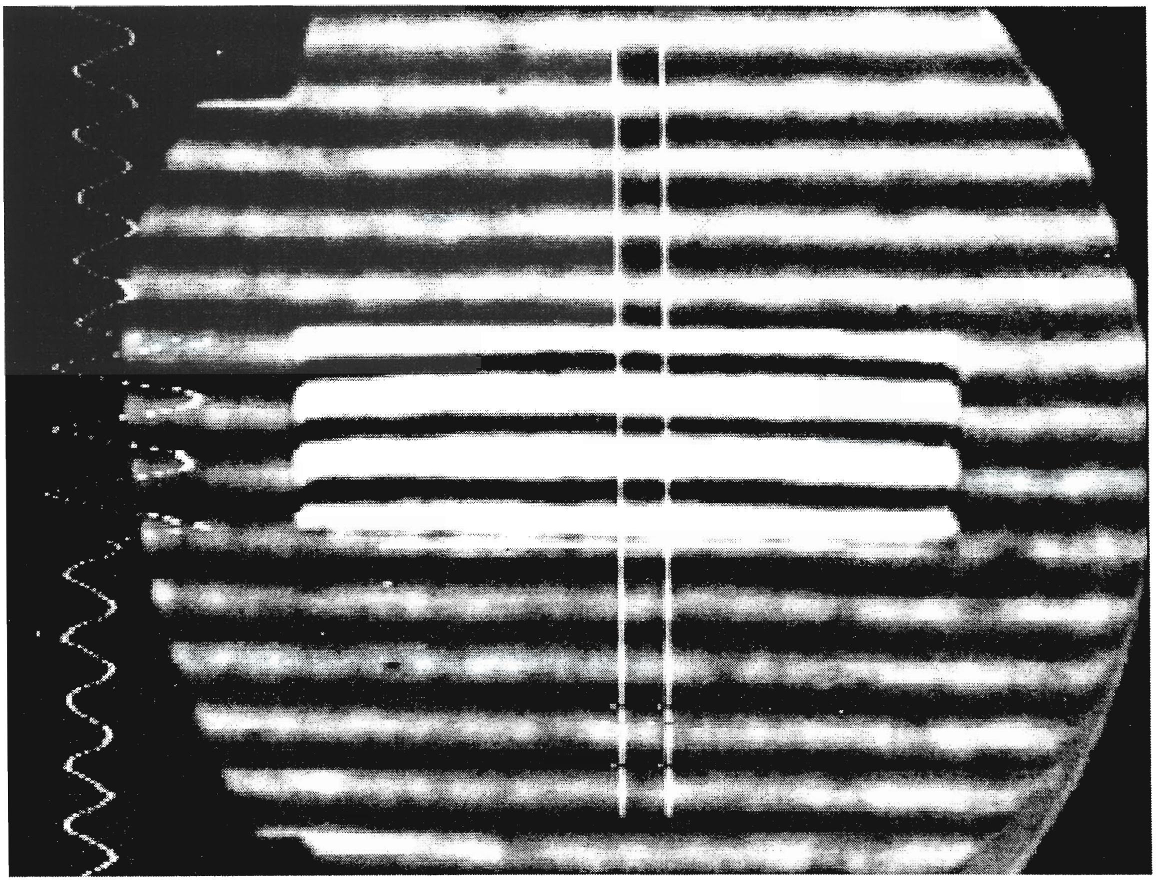

**Figure 2.6** Interferogram obtained by placing the FTG within the GBI

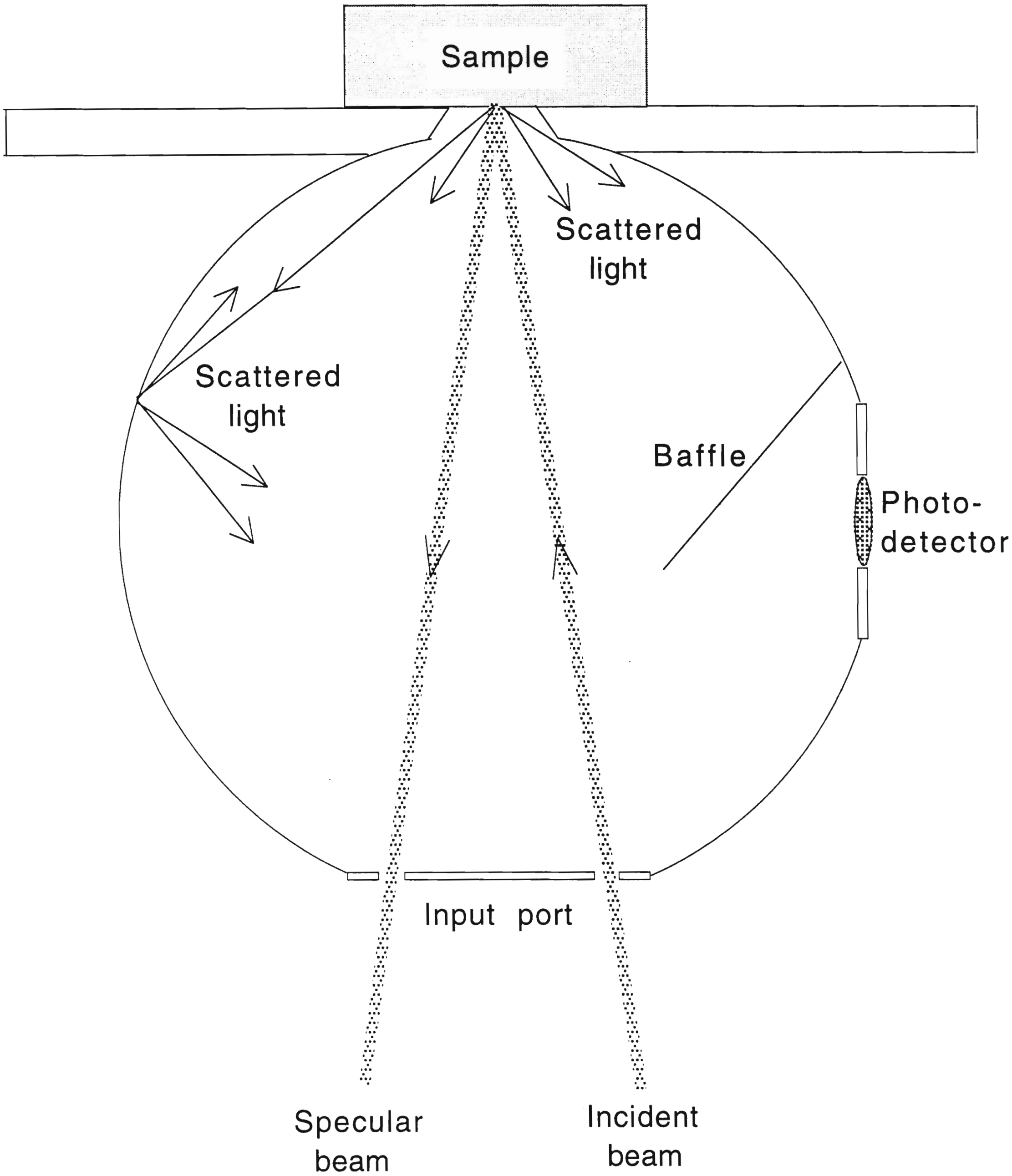


**Figure 3.1** Inside geometry and layout of the integrating sphere

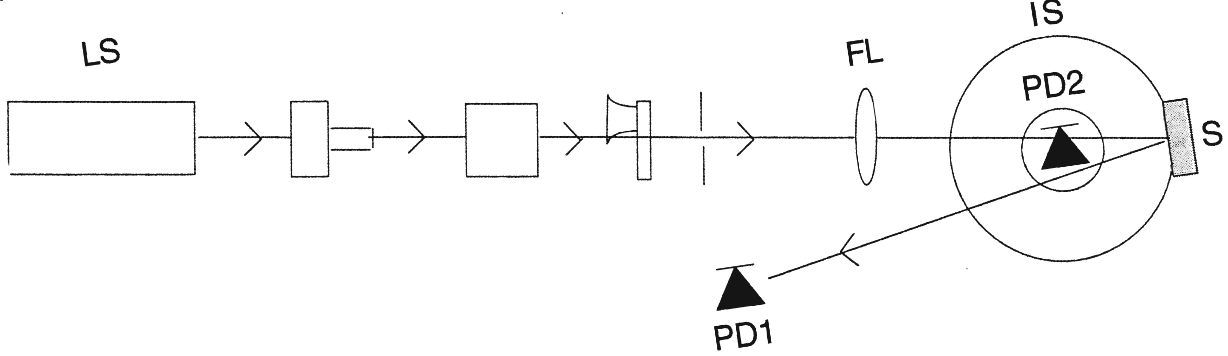


**Figure 3.2** Optical set-up (annotations are described in the accompanying text)

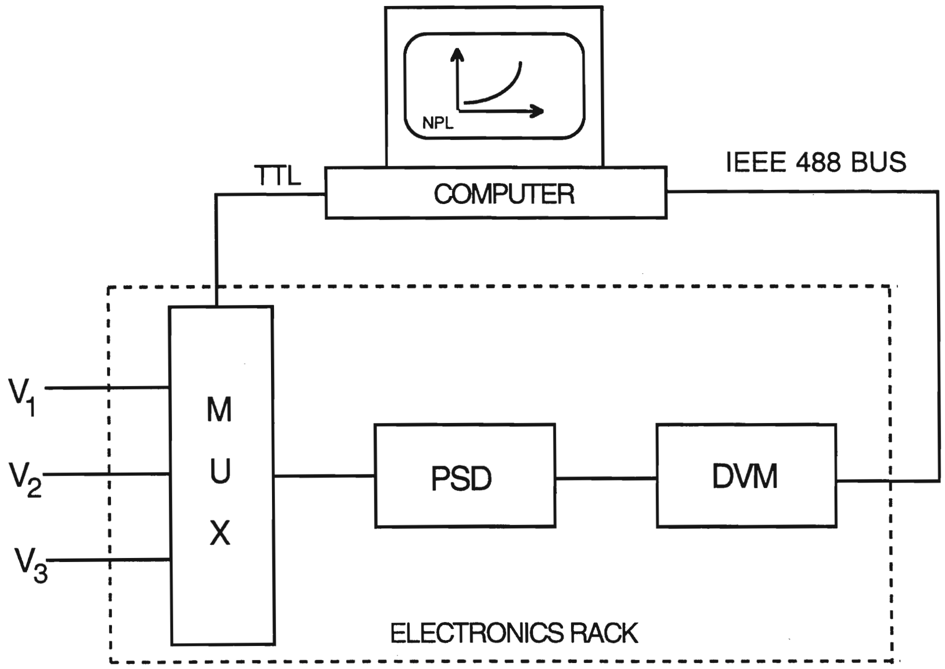


**Figure 3.3** Block diagram of the instrumentation for the final-stage TIS instrument

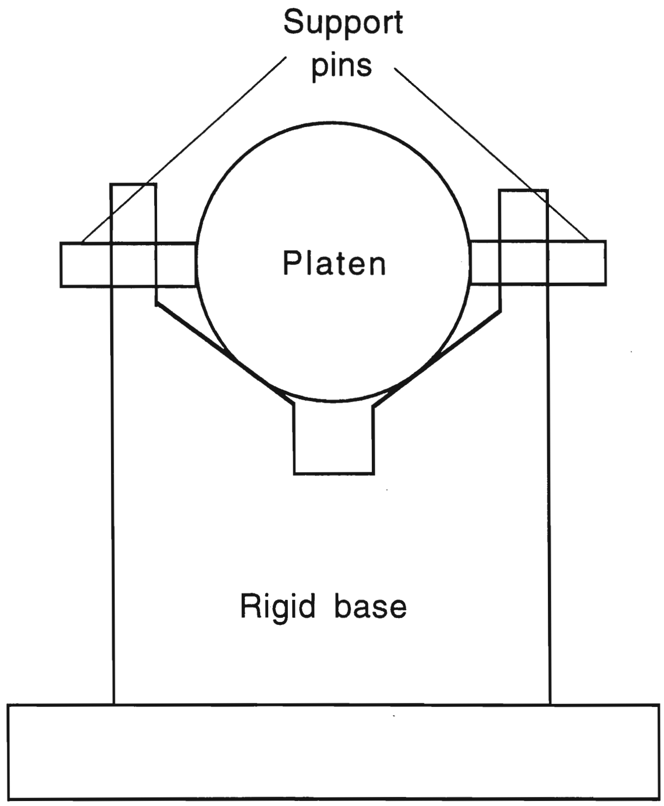


**Figure 4.1** Reference platen for wringing experiments

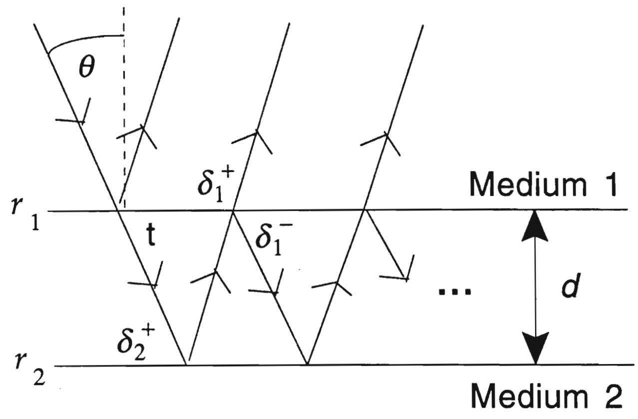


**Figure A.1** A Fizeau cavity (effects due to refraction are not shown)

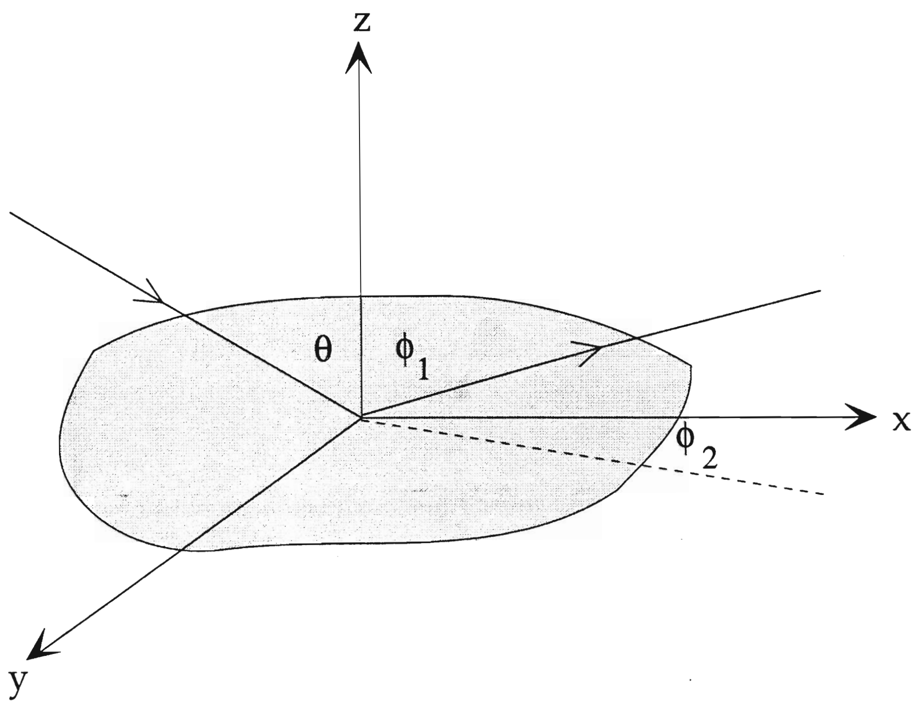


**Figure B.1** Angles of incidence and reflection